RSC Advances

ROYAL SOCIETY OF CHEMISTRY

www.rsc.org/advances

Electronic and optical properties of silicene nanomeshes

Xue-Sheng Ye,[a] Zhi-Gang Shao,*[a] Hongbo Zhao,[a] Lei Yang,[b] and Cang-Long Wang[b]

Received Xth XXXXXXXXXX 20XX, Accepted Xth XXXXXXXXX 20XX
First published on the web Xth XXXXXXXXXX 200X
DOI: 10.1039/b000000x

We have investigated the electronic and optical properties of silicene nanomeshes (SNMs) using first-principle calculations. Emerging information indicates that the resulting properties are sensitive to the width (W) of silicon chains between neighboring holes. Our results show that the bandgaps of SNMs with odd W remain closed. On the contrary, bandgaps are opened in SNMs with even W at the Γ points. Most importantly, SNMs possess broad frequency photoresponse ranging from far infrared (0 eV) to ultraviolet (10 eV) and the optical properties of SNMs can be tuned by varying the value of W. Our results reveal that SNMs, the silicon-based materials, have significant potential for electronic, photonic, and photovoltaic applications.

1 Introduction

Graphene, one of the most promising carbon-based materials with abound of potential applications, has been extensively studied since it was first obtained by Novoselov *et al.*[1,2], but cannot be used in transistor architectures because it is a semimetal with the closed bandgap.[3–6] As a sequence, currently there is a surge in attempts to open a bandgap to make semimetallic graphene suitable for electronic applications, including being cut into nanoribbons,[7–9] being applied transverse electric field[10–13] and absorbing atoms in a regular pattern,[14–19] while these methods meet particular nanotechnology challenges. Recently, graphene antidot lattices (*i.e.* graphene nanomeshes) have been first proposed by Pedersen *et al.*[20] as a strategy to open the bandgap of graphene around the Fermi level. Since then, graphene nanomeshes have been extensively explored.[3–5,5,6,20–30] Previous results show the opened gap is associated with the size, shape, and symmetry of nanomeshes.[5,20–25,31,32] Exhilaratingly, essential experimental progresses of graphene nanomeshes have been achieved. Graphene nanomeshes have been successfully fabricated via the electron beam lithography, block copolymer lithography, and self-assembling of mono-disperse colloidal microspheres.[4,33–37]

Notably, Si as a fundamental material has been the key role in modern electronics industries. However, in photovoltaic industries Si with a indirect bandgap of 1.1 eV[38] can not be made use of the energy below the gap.[39] In addition, the carriers mobilities of Si are not balanced. The electron mobility (1400 $cm^2v^{-1}s^{-1}$) is much larger than the hole mobility (450 $cm^2v^{-1}s^{-1}$).[40,41] The unbalanced charge-transport property results in holes accumulation[42] in Si solar cell devices. Consequently, it reduces the photon to current conversion efficiency[43]. Recently, silicene, the silicon-based counterpart of graphene with the linear dispersion of the band structure at Fermi level, has been investigated quite intensively. Its extremely high carrier mobility makes it an ideal material, especially in electronic devices.[44–50] It is useful for photovoltaic materials that the mobilities of the hole and electron of silicene are in an order of magnitude ($10^5 cm^2v^{-1}s^{-1}$).[51] The more balanced transport of holes and electrons results in better device performance.[43] However, the pristine silicene is similar to the graphene that lacks a band gap which is a necessary condition for its usage in transistor architectures.[3–6,28,52]

Therefore, in this work we introduce periodic holes in silicene to form the silicene nanomeshes (SNMs) by first-principle calculations. And then, we explore the electronic and optical properties of SNMs via density functional theory.

2 Model and methods

The SNMs with periodic hexagonal silicon chains removed are shown in Fig. 1. The rhombus represents the super cell of SNMs. The W indicates the width of the silicon chains between the neighbouring holes. Each type of SNMs is defined with the one removed hexagonal silicon chains (1) and the width (W) of the silicon chains between neighboring holes as {1,W}.[21] The dangling bonds are passivated by hydrogen. In the structure the yellow and gray atoms stand for silicon and hydrogen, respectively. The structural optimizations, band structures and optical spectra were calculated by first-principle calculations via the CASTEP code[53–57] with the periodic boundary conditions. The generalized gradient approximation (GGA) within the Perdew-Burke-Emzerhof

[a] *Laboratory of Quantum Engineering and Quantum Materials, SPTE, South China Normal University, Guangzhou 510006, China E-mail:zgshao@scnu.edu.cn*
[b] *Institute of Modern Physics, Chinese Academy of Sciences, and Department of Physics, Lanzhou University, Lanzhou 730000, China*

(PBE) exchange-correlation functional [58] is employed to describe the exchange and correlation potentials. The vanderbilt ultrasoft pseudopotential [59] is used in the reciprocal space. The energy cutoff for the plane-wave expansion is set to 260 eV and 400 eV for band structure and optical spectra calculations, respectively. The Monkhorst-Pack *k*-point mesh [60] of $21 \times 21 \times 1$ is set to provide sufficient accuracy in the Brillouin-zone integration. SNMs planes are separated by the vacuum of 16 $\AA$ in our calculations to avoid the effect of layers.

In CASTEP calculations, the local field is not considered, so excitonic effects are not taken into account. [53–57] The imaginary part of the dielectric constant, which can be expressed as

$$\varepsilon_2(\mathbf{q} \to O_{\hat{u},h\omega}) = \frac{2e^2\pi}{\Omega\varepsilon_0} \sum_{\mathbf{k},v,c} \left|\langle \Psi^c_{\mathbf{k}} | \mathbf{u}\cdot\mathbf{r} | \Psi^v_{\mathbf{k}} \rangle\right|^2 \delta(E^c_{\mathbf{k}} - E^v_{\mathbf{k}} - E)$$

where Ω and ε_0 are the volume of the super cell and the dielectric constant of the free space, respectively. c and υ represent the conduction band and valence band, respectively. **u** and **r** indicate the polarization direction of the electric field and position vector, respectively. The sum over **k** samples the whole region of Brillouin zone (BZ) in the **k** space. $\varepsilon_2(\omega)$ is calculated by summing all transitions between occupied and unoccupied electronic states over the Brillouin zone. [61,62] Since the real and imaginary parts are linked by a Kramers-Kronig transform, the real part of the dielectric function $\varepsilon_1(\omega)$ can be obtained from $\varepsilon_2(\omega)$. Actually, as long as these two quantities $\varepsilon_1(\omega)$ and $\varepsilon_2(\omega)$ are obtained, the absorption coefficient η can be evaluated via the formula ($\eta = \frac{2\kappa\omega}{c}$), where c is the speed of light and κ is the imaginary part of refractive index($\kappa = (\frac{\sqrt{\varepsilon_1^2+\varepsilon_2^2}-\varepsilon_1}{2})^{\frac{1}{2}}$). In this work, we calculate the optical properties under unpolarized (U) and polarized (P) light conditions. $E_{\parallel}$ polarization is defined if the electric field is parallel to the SNMs and $E_{\perp}$ polarization is defined if the electric field is perpendicular to the SNMs. [63–65] We have only calculated in-plane absorption since SNMs are two-dimensional materials which are discontinuous in the perpendicular direction [65].

3 Results and discussion

Figure 2 illustrates the band structures of SNMs calculated by the CASTEP code [53–57]. After introducing holes in silicene, the symmetry of the unit cell of the SNMs with odd W is reduced from P-3M1 (silicene) to P-3. However, the space group of SNMs with even W changes from P-3M1 (silicene) to P-31M. But they still belong to hexagonal groups. So the area surrounded by the $\Gamma - M - K - \Gamma$ path is the irreducible Brillouin zone of the two dimensional SNMs. As expected, the ones with even W have opened bandgaps (0.64 eV and 0.32eV for {1.2} and {1,4} SNMs, respectively) around the Fermi level at the Γ points as shown in Figs. 2(b) and 2(d). As we know, hydrogen passivation has significant influence on the defects of silicene [66], but Pedersen *et al.* have proved the antidot lattice, the regular holes in the graphene sheet, has the important consequence that the size of the gap can be tuned via the antidote lattice parameters and the periodic perturbation turns the semimetal into a semiconductor. [20] Compared to the odd value of W, it is found that SNMs with even W are partially broken the translational symmetry and the Dirac points are hybridized by the perforation and passivated hydrogen, [4,28,66–68] which lead to gaps. [5,20–25,31,32,69,70] Hence, the energy gap opened in SNMs results from the combination of quantum confinement and the periodic perturbation potential. [22,25–28,69,70] Consequently, SNMs have significant potential to be used as a transistor in logic applications and the small bandgap may be exploited to make new photonic devices for far infrared light detection. On the contrary, the ones with odd W remain semimetallic with Dirac cones in Brillouin zone as shown in Figs. 2(a) and 2(c). Ouyang *et al.* have discussed the closed bandgap at the K point is related to topological connection (bonding) between carbon atoms for graphene nanomeshes. [21] In addition, the modulation behavior of band gap as a function of W in SNMs is similar to that in graphene nanomeshes [21]. Furthermore, we note that silicene has linearly dispersing electronic band structure at the Fermi

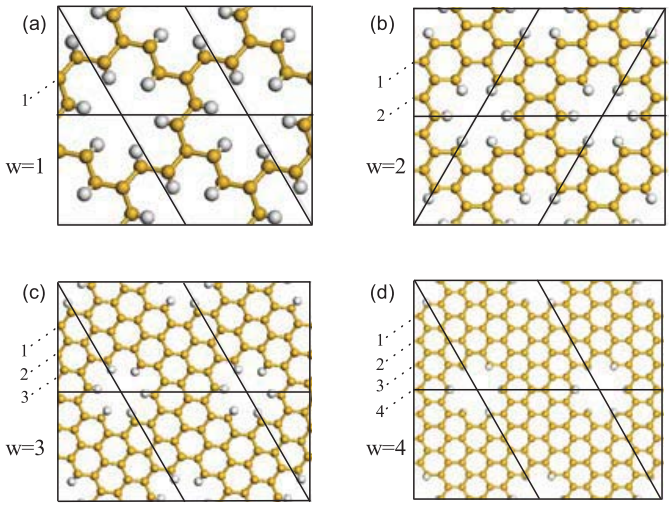

Fig. 1 Structures of silicene nanomeshes (SNMs) with varying width W of the silicon chains between the neighbouring holes labeled as {1,1}(a), {1,2}(b), {1,3}(c), and {1,4}(d). The 1 in {1,W} represents a hexagonal silicon chains removed in SNMs. In the structure the yellow and gray atoms stand for silicon and hydrogen, respectively. The number of the dash lines in Fig. 1(d) illustrates the value of W.

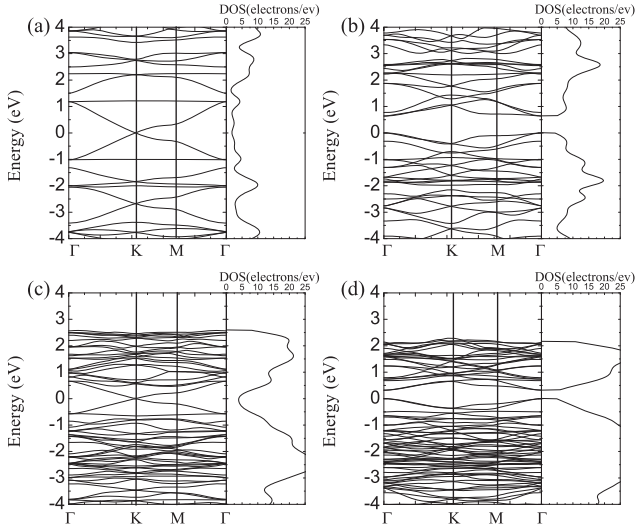

Fig. 2 Band structure and density of states (DOS) of SNMs with {1,1}(a), {1,2}(b), {1,3}(c), and {1,4}(d).

level, which contribute to its high carrier mobility. [51] Though the introduced nanomeshes in silicene would reduce the mobilities of silicene, the valence band and conduction band still preserve symmetry and linear dispersion around the Fermi level as shown in Fig. 2. In this case, the high mobilities will still preserve well in SNMs. Moreover, materials with higher mobilities can extremely improve better device performance.

Figure 3 shows the imaginary part of the dielectric function $\varepsilon_2(\omega)$ of SNMs. A striking difference between the optical spectra of SNMs and Si is that not only for the polarized light but also for the non-polarized light the ε_2 of SNMs take nonzero values from the frequency of 0 eV, compared with that of Si take a nonzero value from the frequency of 1.1 eV which is the threshold for direct optical transitions between the valence band maximum and the conduction band minimum. [71] In Figs. 3(a) and 3(b) the maximum values of $\varepsilon_2(\omega)$ for the four types of SNMs lie within the visible to infrared part of the spectrum$(< 1eV)$, and their peak positions not noticeable change for the unpolarized and the $E_{\|}$ polarized light. But for the $E_{\|}$ polarization the height of the maximum values of $\varepsilon_2(\omega)$ doubled compared with the non-polarization. However, the strong anisotropy in imaginary part of dielectric function is observed under $E_{\|}$ and $E_{\perp}$ polarization conditions. In case of $E_{\perp}$ polarization for the four types of SNMs, the maximum values of $\varepsilon_2(\omega)$ shift to very high frequency region $(\sim 8eV)$, while SNMs with W = 2, 3 and 4 falls to zero in the high frequency region.

The real part of dielectric function $\varepsilon_1(\omega)$ is shown in Fig. 4. It is found that Figs. 4(a) and 4(b) also show the same change tendency of the $\varepsilon_1(\omega)$ ranging from 0 eV to 6 eV, but

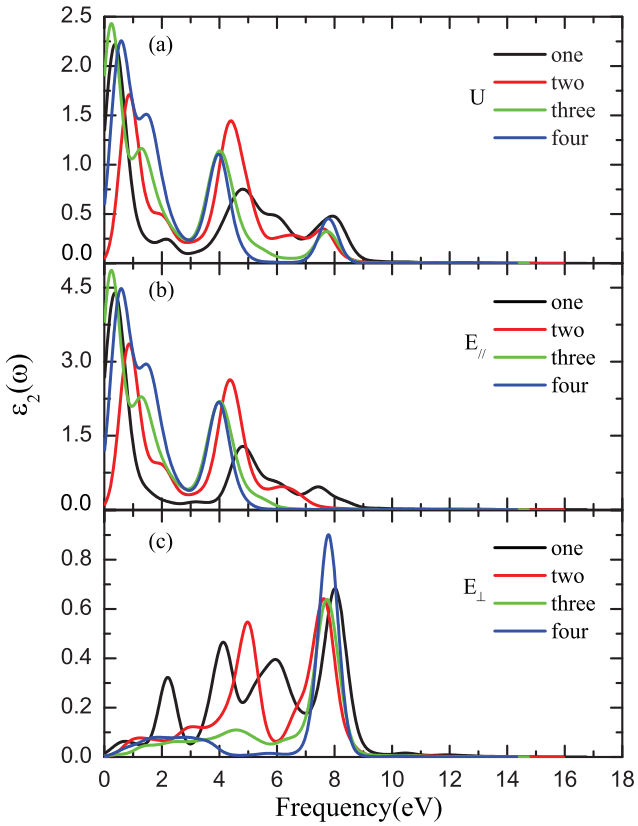

Fig. 3 Imaginary part of the dielectric function $\varepsilon_2(\omega)$ of SNMs for unpolarized (U) and $E_{\|}$ and $E_{\perp}$ polarization (P) light. The black, red, green, and blue lines correspond to {1,1}, {1,2}, {1,3}, and {1,4}, respectively.

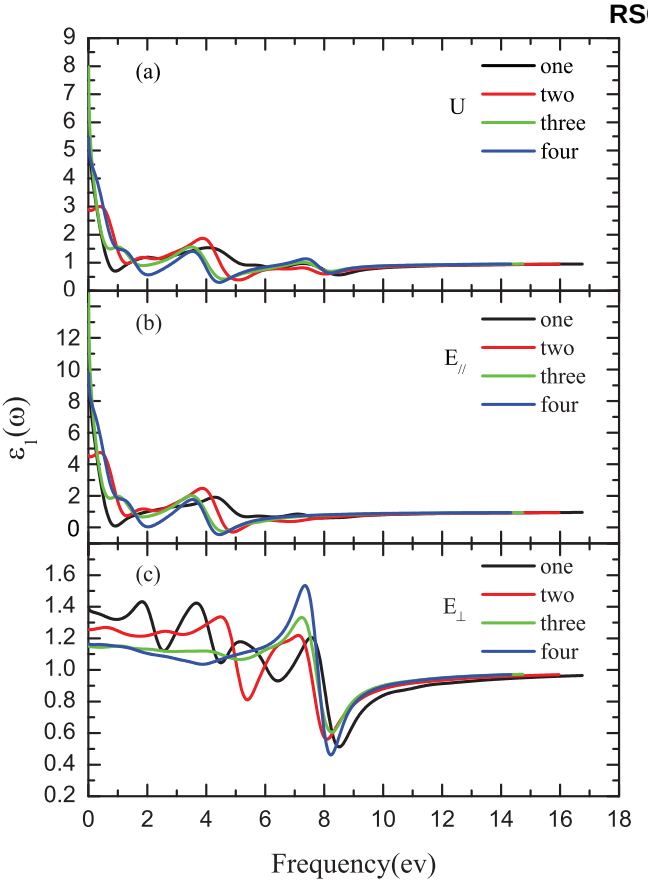

Fig. 4 Real part of the dielectric function $\varepsilon_1(\omega)$ of SNMs for unpolarized (a) and $E_{\parallel}$ (b) and $E_{\perp}$ (c) polarization light. The black, red, green, and blue lines correspond to {1,1}, {1,2}, {1,3}, and {1,4}, respectively.

the values of $\varepsilon_1(\omega)$ in Fig. 4(b) are higher than the ones in Fig. 4(a) under the polarized condition as well. One important quantity of $\varepsilon_1(\omega)$ is the zero frequency limit $\varepsilon_1(0)$, which represents the dielectric response to the static electric field. Figs. 4(a) and 4(b) show the inverse relationship between the band gap and $\varepsilon_1(0)$. A smaller energy gap yields a larger $\varepsilon_1(0)$ value.[71,72] This can be understood based on the expression $\varepsilon_1(0) = 1 + (\frac{\hbar\omega_p}{E_g})^2$.[71,72] In Fig. 4(b), $\varepsilon_1(0)$ describes the varying values ranging from 4.56 to 14.81 for the four types of SNMs under the polarized condition. The higher value of the static dielectric constants leads to larger available free charge carriers.[61] For example, in Fig. 4(b) under the $E_{\parallel}$ polarization condition the two types of SNMs ({1,1} and {1,3}) with Dirac points have the two higher values of 11.51 and 14.81, respectively. However, SNMs with $W = 2$ is a semiconductor with the larger bandgap about 0.64 eV, corresponding $\varepsilon_1(0)$ for $E_{\parallel}$ polarized light is the lower value of 4.56.

Figure 5 describes the absorption spectrum, which indicate

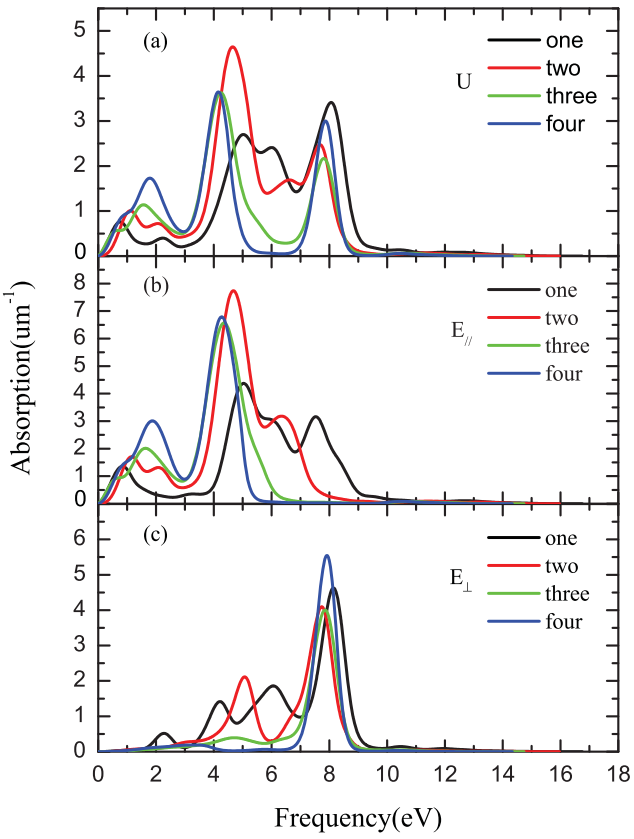

Fig. 5 Absorption coefficient of SNMs for unpolarized (a) and $E_{\parallel}$ (b) and $E_{\perp}$ (c) polarization light. The black, red, green, and blue lines correspond to {1,1}, {1,2}, {1,3}, and {1,4}, respectively.

the fraction of energy lost by the light wave when it passes through the material.[57] It is clearly found that the absorption coefficients of the four types of SNMs take nonzero values from 0 eV under the $E_{\parallel}$ polarization and unpolarized light conditions. They absorb light of different frequencies as W varies. It is obvious that the absorption spectrum below 1 eV more intuitively correspond to the band structure of the four types of the SNMs around the Fermi level. SNMs with odd W reserve the Dirac cones, but their Dirac cones with larger W become more flat showed in Figs. 2(a) and 2(c). The bandgap of SNMs decreases as the value of even W increases. So red shift appears in the absorption spectrum of SNMs with W = 3 compared with the one with W = 1 and the one with W=4 compared with the one with W = 2. In Fig. 5 (a) under the unpolarized light condition the four types of SMNs have three prominent peaks around 2 eV, 4.5 eV, and 8 eV, respectively. The first peak of the four types all starts from 0 eV to the visible light zone, and the peak values locate from 1 eV to 2 eV as corresponding W varies from 1 to 4. In Fig. 5 (b) for the $E_{\parallel}$ polarization light the four types of SNMs lack the third peak in Fig. 5 (a). However, under the $E_{\perp}$ polarization condition the four types of SNMs preserve only the third prominent peak around 8 eV. In Figs. 5(a), 5(b) and 5(c) it is easy to be found that the absorption spectrum are enhanced under the polarization compared with the non-polarization. But SNMs prefer to absorb the $E_{\parallel}$ polarized light below 6 eV, while for the $E_{\perp}$ polarized light SNMs only absorb the light around 8 eV.

Moreover, Figs. 3, 4, and 5 all reveal that optical properties of SNMs are sensitive to the value of W. Our results show that SNMs possess broad frequency photoresponse ranging from 0 eV to 10 eV. We note that a limitation in Si is that it has a band gap of 1.1 eV which means photons with energy below the bandgap are lost.[39,73] Nevertheless, the SNMs can make full use of the solar energy below 1.1 eV. If the SNMs-based solar cell can be developed, the utilization of sunlight will be extremely improved. And SNMs can be exploited to make new photonic devices for far infrared light detection with the absorption from 0 eV.[65] In addition, strong anisotropy in the optical properties is also observed contrasted with that Si is optically isotropic. The polarized dependent optical spectra would make the SNMs more versatile than Si in potential applications.

4 Conclusions

In summary, we have investigated the electronic and optical properties of SNMs. Our results show that the electronic and optical properties of SNMs are extremely sensitive to the W of silicon chains between the neighboring holes. The bandgap of SMNs with odd W remains closed. On the contrary, substantial bandgaps are opened in SMNs with even W around the Fermi level. Hence, SNMs have significant potential for applications in electronics, and the SNMs with even W, which is a semiconductor, can be used for effective field-effect transistors operating at the room temperature. SNMs also can be exploited to make new photonic devices for far infrared light detection with the absorption from 0 eV. In addition, our results show the optical properties of SNMs are anisotropy under $E_{\parallel}$ and $E_{\perp}$ polarized conditions. Furthermore, the optical properties of SNMs can be tuned by varying W. SNMs, possessing broad frequency photoresponse ranging from 0 eV to ultra-violet region 10 eV, can be made good use for solar energy. Since photovoltaics can make a considerable contribution to solving the energy problem that our society faces,[39] SNMs may pave a possible way towards solar cell materials.

Acknowledgement

Zhi-Gang Shao acknowledges the support by the National Natural Science Foundation of China (Grant Nos. 11105054 and 11274124), PCSIRT (Grant No. IRT1243), China Scholarship Council, and by the high-performance computing platform of South China Normal University. Hongbo Zhao acknowledges the support by the National Natural Science Foundation of China (Grant No. 91026005). Lei Yang acknowledges the support by the "Strategic Priority Research Program" of the Chinese Academy of Sciences (Grant No. XDA03030100). Cang-Long Wang acknowledges the support by the National Natural Science Foundation of China (Grant No. 11304324).

References

1 K. S. Novoselov, A. K. Geim, S. V. Morozov, D. Jiang, Y. Zhang, S. V. Dubonos, I. V. Grigorieva and A. A. Frisov, *Science*, 2004, **306**, 666–669.
2 K. S. Novoselov, A. K. Geim, S. V. Morozov, D. Jiang, M. I. Katsnelson, I. V. Grigorieva, S. V. Dubonos and A. A. Frisov, *Nature*, 2005, **438**, 197.
3 R. Martinazzo, S. Casolo and G. F. Tantardini, *Phys. Rev. B*, 2010, **81**, 245420.
4 J. Bai, X. Zhong, S. Jiang, Y. Huang and X. Duan, *Nat Nano*, 2010, **5**, 190–194.
5 R. Petersen, T. G. Pedersen and A.-P. Jauho, *ACS Nano*, 2011, **5**, 523–529.
6 S. Yuan, R. Roldán, A.-P. Jauho and M. I. Katsnelson, *Phys. Rev. B*, 2013, **87**, 085430.
7 M. Y. Han, B. Özyilmaz, Y. Zhang and P. Kim, *Phys. Rev. Lett.*, 2007, **98**, 206805.
8 Y.-W. Son, M. L. Cohen and S. G. Louie, *Phys. Rev. Lett.*, 2006, **97**, 216803.
9 L. Brey and H. A. Fertig, *Phys. Rev. B*, 2006, **73**, 235411.
10 E. V. Castro, K. S. Novoselov, S. V. Morozov, N. M. R. Peres, J. M. B. L. dos Santos, J. Nilsson, F. Guinea, A. K. Geim and A. H. C. Neto, *Phys. Rev. Lett.*, 2007, **99**, 216802.
11 E. McCann, *Phys. Rev. B*, 2006, **74**, 161403.
12 A. Deshpande, W. Bao, Z. Zhao, C. N. Lau and B. J. LeRoy, *Appl. Phys. Lett.*, 2009, **95**, 243502.

13 Z. Ni, Q. Liu, K. Tang, J. Zheng, J. Zhou, R. Qin, Z. Gao, D. Yu and J. Lu, *Nano Lett.*, 2012, **12**, 113–118.

14 R. Balog, B. Jorgensen, L. Nilsson, M. Andersen, E. Rienks, M. Bianchi, M. Fanetti, E. Laegsgaard, A. Baraldi, S. Lizzit, Z. Sljivancanin, F. Besenbacher, B. Hammer, T. G. Pedersen, P. Hofmann and L. Hornekaer, *Nat Mater*, 2010, **9**, 315–319.

15 J. O. Sofo, A. S. Chaudhari and G. D. Barber, *Phys. Rev. B*, 2007, **75**, 153401.

16 L. Liu and Z. Shen, *Appl. Phys. Lett.*, 2009, **95**, 252104.

17 X.-L. Wei, H. Fang, R.-Z. Wang, Y.-P. Chen and J.-X. Zhong, *Appl. Phys. Lett.*, 2011, **99**, 012107.

18 X. Liu, Y. Wen, Z. Chen, H. Lin, R. Chen, K. Cho and B. Shan, *AIP Adv.*, 2013, **3**, 052126.

19 R. Wang, X. Pi, Z. Ni, Y. Liu, S. Lin, M. Xu and D. Yang, *Sci. Rep.*, 2013, **3**, 1–6.

20 T. G. Pedersen, C. Flindt, J. Pedersen, N. A. Mortensen, A.-P. Jauho and K. Pedersen, *Phys. Rev. Lett.*, 2008, **100**, 136804.

21 F. Ouyang, S. Peng, Z. Liu and Z. Liu, *ACS Nano*, 2011, **5**, 4023–4030.

22 J. Lee, A. K. Roy, J. L. Wohlwend, V. Varshney, J. B. Ferguson, W. C. Mitchel and B. L. Farmer, *Appl. Phys. Lett.*, 2013, **102**, 203107.

23 F. Ouyang, Z. Yang, S. Peng, X. Zheng and X. Xiong, *Physica E: Low-dimensional Systems and Nanostructures*, 2014, **56**, 222 – 226.

24 X. Y. Cui, R. K. Zheng, Z. W. Liu, L. Li, B. Delley, C. Stampfl and S. P. Ringer, *Phys. Rev. B*, 2011, **84**, 125410.

25 H. Jippo, M. Ohfuchi and C. Kaneta, *Phys. Rev. B*, 2011, **84**, 075467.

26 M. H. Schultz, A. P. Jauho and T. G. Pedersen, *Phys. Rev. B*, 2011, **84**, 045428.

27 C.-H. Park, L. Yang, Y.-W. Son, M. L. Cohen and S. G. Louie, *Phys. Rev. Lett.*, 2008, **101**, 126804.

28 K. Lopata, R. Thorpe, S. Pistinner, X. Duan and D. Neuhauser, *Chem. Phys. Lett.*, 2010, **498**, 334 – 337.

29 W. Oswald and Z. Wu, *Phys. Rev. B*, 2012, **85**, 115431.

30 H. Şahin and S. Ciraci, *Phys. Rev. B*, 2011, **84**, 035452.

31 J. A. Fürst, T. G. Pedersen, M. Brandbyge and A.-P. Jauho, *Phys. Rev. B*, 2009, **80**, 115117.

32 H. Y. He, Y. Zhang and B. C. Pan, *J. Appl. Phys.*, 2010, **107**, 114322.

33 M. Kim, N. S. Safron, E. Han, M. S. Arnold and P. Gopalan, *Nano Letters*, 2010, **10**, 1125–1131.

34 X. Liang, Y.-S. Jung, S. Wu, A. Ismach, D. L. Olynick, S. Cabrini and J. Bokor, *Nano Letters*, 2010, **10**, 2454–2460.

35 T. Shen, Y. Q. Wu, M. A. Capano, L. P. Rokhinson, L. W. Engel and P. D. Ye, *Appl. Phys. Lett.*, 2008, **93**, 122102.

36 S. Heydrich, M. Hirmer, C. Preis, T. Korn, J. Eroms, D. Weiss and C. Schüller, *Appl. Phys. Lett.*, 2010, **97**, 043113.

37 A. Sinitskii and J. M. Tour, *J. Am. Chem. Soc.*, 2010, **132**, 14730–14732.

38 J. D. Holmes, K. P. Johnston, R. C. Doty and B. A. Korgel, *Science*, 2000, **287**, 1471–1473.

39 H. A. Atwater and A. Polman, *Nat Mater*, 2010, **9**, 205–213.

40 G. W. Ludwig and R. L. Watters, *Phys. Rev.*, 1956, **101**, 1699–1701.

41 M. B. Prince, *Phys. Rev.*, 1954, **93**, 1204–1206.

42 C. Melzer, E. J. Koop, V. D. Mihailetchi and P. W. M. Blom, *Adv. Funct. Mater.*, 2004, **14**, 865–870.

43 G. Li, V. Shrotriya, J. Huang, Y. Yao, T. Moriarty, K. Emery and Y. Yang, *Nat Mater*, 2005, **4**, 864–868.

44 P. De Padova, C. Quaresima, C. Ottaviani, P. M. Sheverdyaeva, P. Moras, C. Carbone, D. Topwal, B. Olivieri, A. Kara, H. Oughaddou, B. Aufray and G. Le Lay, *Appl. Phys. Lett.*, 2010, **96**, 261905.

45 B. Lalmi, H. Oughaddou, H. Enriquez, A. Kara, S. Vizzini, B. Ealet and B. Aufray, *Appl. Phys. Lett.*, 2010, **97**, 223109.

46 S. Cahangirov, M. Topsakal, E. Aktürk, H. Şahin and S. Ciraci, *Phys. Rev. Lett.*, 2009, **102**, 236804.

47 C.-C. Liu, W. Feng and Y. Yao, *Phys. Rev. Lett.*, 2011, **107**, 076802.

48 G. G. Guzmán-Verri and L. C. Lew Yan Voon, *Phys. Rev. B*, 2007, **76**, 075131.

49 F.-b. Zheng, C.-w. Zhang, P.-j. Wang and S.-s. Li, *J. Appl. Phys.*, 2013, **113**, 154302.

50 T. P. Kaloni, Y. C. Cheng and U. Schwingenschlögl, *J. Appl. Phys.*, 2013, **113**, 104305.

51 Z.-G. Shao, X.-S. Ye, L. Yang and C.-L. Wang, *J. Appl. Phys.*, 2013, **114**, 093712.

52 M. L. Trolle, U. S. Møller and T. G. Pedersen, *Phys. Rev. B*, 2013, **88**, 195418.

53 M. D. Segall, P. J. D. Lindan, M. J. Probert, C. J. Pickard, P. J. Hasnip, S. J. Clark and M. C. Payne, *J. Phys.: Condens. Matter*, 2002, **14**, 2717.

54 P. Hohenberg and W. Kohn, *Phys. Rev.*, 1964, **136**, B864–B871.

55 W. Kohn and L. J. Sham, *Phys. Rev.*, 1965, **140**, A1133–A1138.

56 M. C. Payne, M. P. Teter, D. C. Allan, T. Arias and J. D. Joannopoulos, *Rev. Mod. Phys.*, 1992, **64**, 1045–1097.

57 S. J. Clark, M. D. Segall, C. J. Pickard, P. J. Hasnip, M. J. Probert, K. Refson and M. Payne, *Z. Kristall.*, 2005, **220**, 567–570.

58 J. P. Perdew, K. Burke and M. Ernzerhof, *Phys. Rev. Lett.*, 1996, **77**, 3865–3868.

59 D. Vanderbilt, *Phys. Rev. B*, 1990, **41**, 7892–7895.

60 J. D. Monkhorst, H. J. Pack, *Phys. Rev. B*, 1976, **13**, 5188–5192.

61 S. Kumar Jain and P. Srivastava, *J. Appl. Phys.*, 2013, **114**, 073514.

62 N. Singh, T. P. Kaloni and U. Schwingenschlögl, *Appl. Phys. Lett.*, 2013, **102**, 023101.

63 J. Kang, J. Li, F. Wu, S.-S. Li and J.-B. Xia, *J. Phys. Chem. C*, 2011, **115**, 20466–20470.

64 Y. Liu, H. Shu, P. Liang, D. Cao, X. Chen and W. Lu, *J. Appl. Phys.*, 2013, **114**, 20466–20470.

65 L. Matthes, P. Gori, O. Pulci and F. Bechstedt, *Phys. Rev. B*, 2013, **87**, 035438.

66 J. Gao, J. Zhang, H. Liu, Q. Zhang and J. Zhao, *Nanoscale*, 2013, **5**, 9785–9792.

67 T. H. Osborn, A. A. Farajian, O. V. Pupysheva, R. S. Aga and L. L. Y. Voon, *Chem. Phys. Lett.*, 2011, **511**, 101 – 105.

68 E. Bekaroglu, M. Topsakal, S. Cahangirov and S. Ciraci, *Phys. Rev. B*, 2010, **81**, 075433.

69 C.-L. Lin, R. Arafune, K. Kawahara, M. Kanno, N. Tsukahara, E. Minamitani, Y. Kim, M. Kawai and N. Takagi, *Phys. Rev. Lett.*, 2013, **110**, 076801.

70 Y.-L. Song, Y. Zhang, J.-M. Zhang, D.-B. Lu and K.-W. Xu, *J. Mol. Struct.*, 2011, **990**, 75 – 78.

71 L. Guo, S. Zhang, W. Feng, G. Hu and W. Li, *J. Alloy. Compd.*, 2013, **579**, 583 – 593.

72 D. R. Penn, *Phys. Rev.*, 1962, **128**, 2093–2097.

73 C. Solanki and G. Beaucarne, *Energy Sustain. Dev.*, 2007, **11**, 17 – 23.